Solid Freeform Fabrication 2023: Proceedings of the 34th Annual International Solid Freeform Fabrication Symposium – An Additive Manufacturing Conference
Reviewed Paper

Oxide Dispersion Strengthened (ODS) SS316L Prepared by Laser Powder Bed Fusion (L-PBF): Analysis of Microstructure and Hardness Properties

Changyu Ma[1,2], Yu-Keng Lin[2,3], Tianqi Zheng[2,4], Philip Mallory[5], Jianhao Zhu[1,2], Y. Morris Wang[3], Xiaochun Li[4], Bruce Kang[5], Bingbing Li[1,2]*

[1]Autonomy Research Center for STEAHM (ARCS), California State University, Northridge, CA 91324
[2]Terasaki Institute for Biomedical Innovation, Los Angeles, CA 90024
[3]Department of Material Science and Engineering, University of California Los Angeles, Los Angeles, CA 90095
[4]Department of Mechanical and Aerospace Engineering, University of California Los Angeles, Los Angeles, CA 90095
[5]Department of Mechanical and Aerospace Engineering, West Virginia University, Morgantown, WV 26506

Correspondence: bingbing.li@csun.edu

Abstract

In this paper, dense oxide dispersion-strengthened (ODS) SS316L with 0.5 wt.% Y_2O_3 was fabricated using nano-Y_2O_3-embedded spherical SS316L powder via laser powder bed fusion (L-PBF). The molten pool, oxide dispersion, cellular structure, and microhardness of the as-printed ODS SS316L were investigated through optical microscopy (OM), scanning electron microscopy (SEM), energy dispersive X-Ray Spectroscopy (EDX), and Vickers hardness testing, respectively. The results reveal a uniform dispersion of Y-rich nanoparticles in as-printed ODS SS316L, contributing to the development of a fine-grain structure in the as-printed ODS SS316L. A wide and shallow molten pool was observed in as-printed ODS SS316L, and enhanced microhardness was observed in ODS SS316L compared to pristine SS316L. The effects of Y_2O_3 on microstructure evolution and reinforcing mechanisms of microhardness are discussed.

Keywords: ODS SS316L, Y_2O_3, additive manufacturing, grain refinement

1. Introduction

Austenitic stainless steel 316L (SS316L) is widely used in industries such as jet engines, heat exchangers, and biomedicine due to its excellent ductility, corrosion resistance, and biocompatibility. Solution-annealed SS316L has been considered the most suitable material for irradiation resistance under relatively high loads and direct contact with water.[1] Additionally, the development of oxide dispersion strengthened (ODS) steels is a key approach to overcoming irradiation-induced swelling using conventional powder metallurgy (PM), with the inclusion of highly stable Y_2O_3 nanoparticles. [2] The minor percentage, typically less than 1.5 wt.%, of oxides requires a uniform distribution of oxide particles in metal matrix to retain optimized strengthening effects, and incorporation of refractory elements, such as hafnium, plays an important role in oxide refinement. [3] However, there are currently several challenges in producing ODS SS316L through conventional PM, including high labor costs, difficulties in manufacturing complex geometries, and long lead times. Therefore, a novel process is required to meet the demands for customized or advanced designs of ODS SS316L components.

Recent advances in additive manufacturing (AM) offer an alternative way to produce oxide dispersion strengthened (ODS) materials with their layer-by-layer processing ability. Although AM has been utilized in the fabrication of porous ODS-free alloys structures [4, 5], producing

ODS alloys is the main challenge since the lack of suitable powder feedstock. [6] In the past few years, exploration of AM-fabricated ODS SS316L have been conducted using mixture of commercial SS316L and Y_2O_3. Zhong et al. [7] reported improved strength and ductility of SS316L fabricated by EOS M270 with ball-milled powder feedstock, achieving a yield strength of 574 MPa and elongation of 91% at room temperature. Grandhi et al. [8] compared 0.5 wt.% Y_2O_3-strengthened and pristine SS316L produced by the DED method, with the results showing a finer grain, higher hardness, and modulus in ODS SS316L. Hu et al. [9] investigated the simultaneous improvement of strength and ductility of L-PBF fabricated SS316L with various Y_2O_3 compositions, achieving a strength of 732 MPa in 0.25 wt.% doped SS316L compared to the original SS316L, owing to the formation of twins, although anisotropy was independent of compositions. While it should be noted that suitable ODS alloys powder for laser powder bed fusion (L-PBF) AM is one of remaining challenges,[6] it is of interest to investigate suitable ODS SS316L powder for L-PBF process, followed by the characterization of as-fabricated ODS SS316L parts.

In this study, we explored the potential of incorporating 0.5 wt.% nano Y_2O_3 particles into spherical SS316L powder for L-PBF AM to achieve dense SS316L using meander and chessboard patterns. We analyzed the morphology of the molten pool, microstructure, and hardness properties using optical microscopy (OM), scanning electron microscopy (SEM), and Vickers' hardness tester. The results demonstrated the successful production of crack-free ODS SS316L using both meander and chessboard printing patterns. The molten pool was found to be layer-dependent, displaying a wide and shadow shape. At the border of the molten pool, a dendritic structure was observed, while near the center of the pool, fine and equiaxed cells were present due to a slower cooling rate compared to the border region. Additionally, the ODS SS316L exhibited enhanced hardness compared to the original SS316L. The strengthening mechanism of ODS SS316L was further discussed.

2. Materials and methods

2.1 Powder preparation

Commercial gas atomized SS316L (Carpenter additive Inc.) with a size range of 15 to 45 μm and Y_2O_3 powders (Sigma Aldrich, size <50 nm) were utilized for powder fabrication. Fine powders were observed on the surface of host SS316L particles, as shown in Figure 1(a) and1(b), suggesting a common satellite surface of gas atomized powder feedstock [10]. Transmission electron microscope (TEM, JEOL JEM-2100 Transmission Electron Microscope) was employed to show particle morphology of nano-sized Y_2O_3, and the high-resolution TEM (HRTEM) image of Y_2O_3 was shown in Fig. 1(c). A novel powder processing technique developed by the author was employed to breakdown and embed nanoparticle onto metal powder surfaces [11], achieving the Y_2O_3-embedded spherical SS316L powder suitable for L-PBF process.

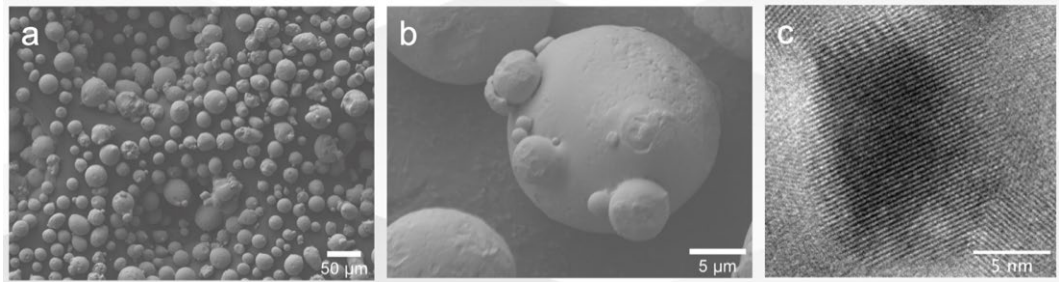

Figure 1. Starting powders. SEM images of SS316L at (a) low magnification and (b) high magnification, (c) HRTEM image of Y_2O_3

2.2 L-PBF process

The rectangular blocks of L-PBF SS316L with a dimension of 32 mm (length) × 13 (width) × 15 mm (height), was built on a mild steel plate by Renishaw AM400 printer equipped with pulsed laser (Figure 2(a)) using reduced build volume mode under argon atmosphere. The oxygen content during the entire printing process was kept less than 1000 ppm. A laser power of 200 Watts, scanning speed of 750mm/s, hatch distance of 110 µm, and layer thickness of 50 µm were utilized for printing, and both chessboard (with size of 5 mm) and meander scanning strategy were utilized in this study (Figure 2(b)).

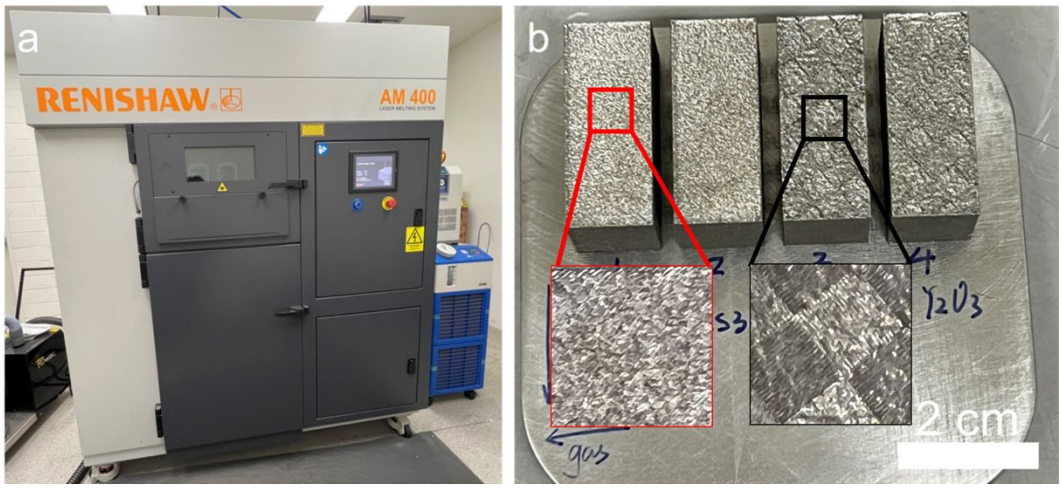

Figure 2. AM printing of ODS SS316L. (a) Renishaw AM400 printer, (b) as printed ODS SS316L, enlarged pictures show the surface morphology of samples printed with meander and chessboard patterns.

2.3 Materials characterization

A field emission scanning electron microscope (SEM, ZEISS SUPRAU 40VP, Carl Zeiss, Jena, Germany) equipped with energy dispersive X-ray spectroscopy (EDS, Thermo Noran System SIX EDS system, Thermo Scientific, USA) was employed to examine the powder morphology and the distribution of yttrium within the powder feedstock at acceleration voltage of 10 KV and working distance of 10 mm. The as-printed blocks were machined from the SS316L substrate using electrical discharge machining (EDM). Subsequently, they were ground with SiC paper up to 1200 grits before being polished using 200-proof ethanol and a 0.05 µm alumina suspension. To reveal the morphology of the molten pool and cellular structure, the block samples were then etched using Marble's reagent. The morphology of molten pool was examined using optical microscopy, then SEM with 10KV acceleration voltage was employed to investigate the microstructure of as-printed ODS SS316L.

2.4 Vickers microhardness testing

The samples were obtained from the as-built blocks using EDM. Prior to hardness testing, the samples were polished with SiC sandpapers down to 1200 metallurgical grits, followed by alumina suspensions to 0.05 µm. The Vickers microhardness values were determined using an LM-800AT microhardness tester (LECO Corporation, Michigan, USA) with 10 s dwell time and 250 gf applied

load. The distances between the indents were set as 0.25 mm, following ASTM E92-17 standard. For statistical analysis, nine data points were averaged to obtain microhardness values. The planes perpendicular/parallel to the building direction were subjected to indentation measurements.

3. Results and discussion

3.1 Powder feedstock

Through the novel powder processing technique, spherical SS316L embedded with nano Y_2O_3 was successfully achieved. Figure 3 presents the morphology and particle size analysis of powder product for laser powder bed fusion (L-PBF) additive manufacturing. In Figure 3(a) and (b), low and high magnification images of the ODS SS316L powder are displayed, showing a smoother surface without fine particles compared to the original SS316L particles shown in Figure 1. Furthermore, Figure 3(b) reveals dense particles without white Y_2O_3 particles on the surface. Figure 3(c) illustrates the particle size distribution ranging from 5 to 40 μm. The increase in particle counts below 15 μm can be attributed to the surface cleaning effects during the powder preparation process, which separates the fine particles (< 15 μm) from host particles.

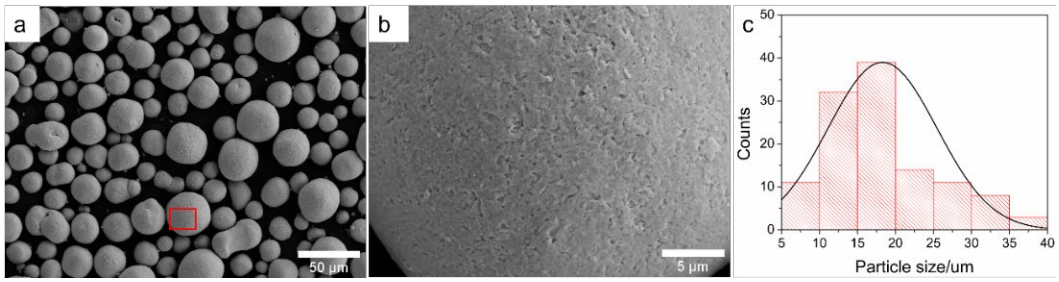

Figure 3. Morphology and size distribution of powder feedstock. (a) SS316L +0.5 wt.% Y_2O_3, (b) surface morphology of circled particle in (a), (c) size analysis of powder product

Figure 4 displays the EDS mapping of chromium, oxygen, and yttrium elements in powder feedstock. It is evident from the mapping that a high content of yttrium and oxygen was detected, with values of 6.44 +/- 0.24, and 1.84 +/- 0.25 wt.%, respectively. The high-density yttrium demonstrates the existence of Y_2O_3 in powder product and the Y_2O_3 particles were expected to be embedded in metal matrix, with no white Y_2O_3 particles observed on powders' surface based on SEM results, as shown in Fig.3(a) and 3(b). The breakdown and dispersion of Y_2O_3 inside metal matrix is owing to the compaction force between powders during powder processing, where ductile and brittle powders are subjected to deformation and breakdown, respectively. The authors also reported Y_2O_3 particles effects on additively manufactured IN718 with the novel powder processing, which enables grain refinement and improvement of ductility of IN718. [12]

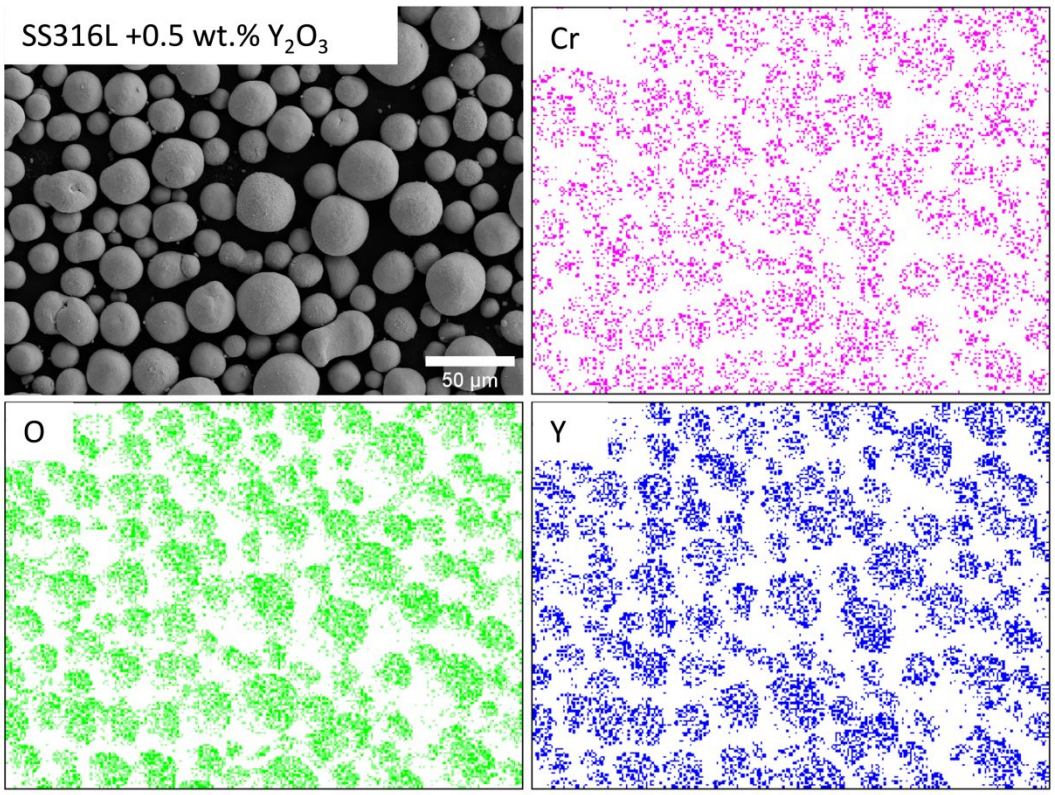

Elements	Fe	Cr	Ni	Y	Mo	O
Wt.%	48.31	19.61	21.79	6.44	2.01	1.84
Wt.% Error	±1.05	±0.58	±0.74	±0.24	±0.24	±0.25

Figure 4. Elements distribution in ODS SS316L powder feedstock

3.2 Morphology of molten pool

In the L-PBF process, the molten pool typically remains in a liquid state when the high-energy laser dwells on a specific spot. It then undergoes rapid cooling when the laser moves to the next spot. Dense ODS SS316L was successfully printed using the standard printing parameters for original SS316L, demonstrating the excellent printing ability of the powder feedstock with embedded nanoparticles. The evolution of oxides in the molten pool can be categorized into two behaviors: breakdown and coarsening. The breakdown of oxides is primarily driven by Marangoni flow, which is the flow of liquid caused by surface tension gradients. This flow helps break down and distribute oxide particles within the molten pool. On the other hand, coarsening occurs due to the lighter density of oxides and poor wettability between the oxides and the metal matrix, resulting in the floating and agglomeration of oxides. In this study, minor agglomeration of oxides was observed along the border of the molten pool, while a uniform distribution of nanoparticles was observed inside the molten pool (as shown in Fig. 5(a)). This suggests different precipitation behaviors of oxides inside the molten pool when Y_2O_3 nanoparticles are embedded in the powder

feedstock. A wide and shallow molten pool was observed, which can be attributed to the Marangoni flow of liquid driven by the surface tension gradient, as shown in Fig. 5(b). A negative value of the surface tension gradient promotes a radial outward flow and leads to a wider and shallower molten pool.[13] It should be noted that the coarsening of oxides caused by uneven liquid flow within the molten pool is a recognized phenomenon in SS 316L [7] and IN718 alloys [14]. The nature of the L-PBF AM process, with its extremely high cooling rates (up to 10^6 K/s), and the addition of oxides in powder matrix call for proper measures to alleviate the issue of oxide coarsening during or after the L-PBF AM process.

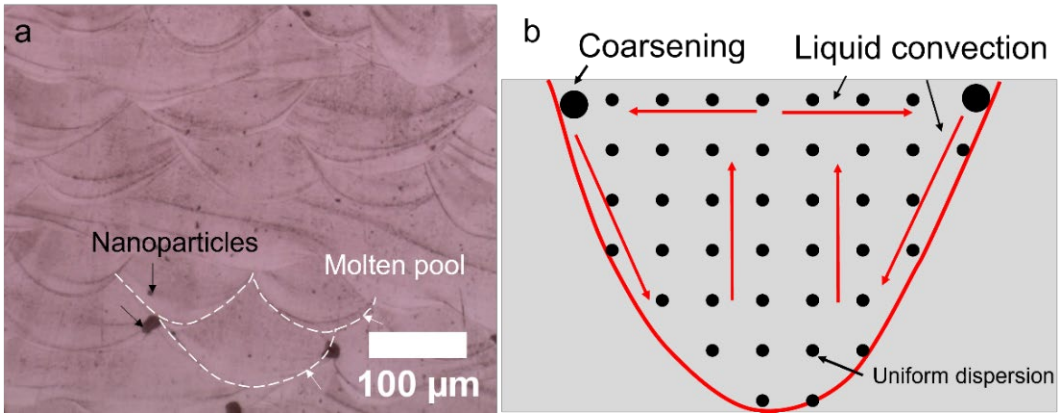

Figure 5. Molten pool of ODS SS316L. (a) Molten pool, (b) schematic of liquid flow

3.3 Cellular structure

In additive manufacturing, the extreme cooling rate favors cellular structure formation and benefits the notable pinning effect for the moment of dislocations. Cui et al. [15] reported improved fatigue performance of additively manufactured SS316L with cellular structures, with a higher strength, lower cyclic softening rate, and longer lifetime benefit from the activation of planar slip. Fig. 6(a) and 6(b) showed the cellular structure and sub grain structure in as-printed ODS SS316L. Nano inclusions were observed inside sub grains and cellular structures, Deng et al. [16] reported oxide inclusions in L-PBF-fabricated SS316L, showing the Si-rich oxides around 100 µm. It should be noted the inclusions are nano-sized and the mechanism of ultrafine oxides formation is unclear with the absence of further characterization.

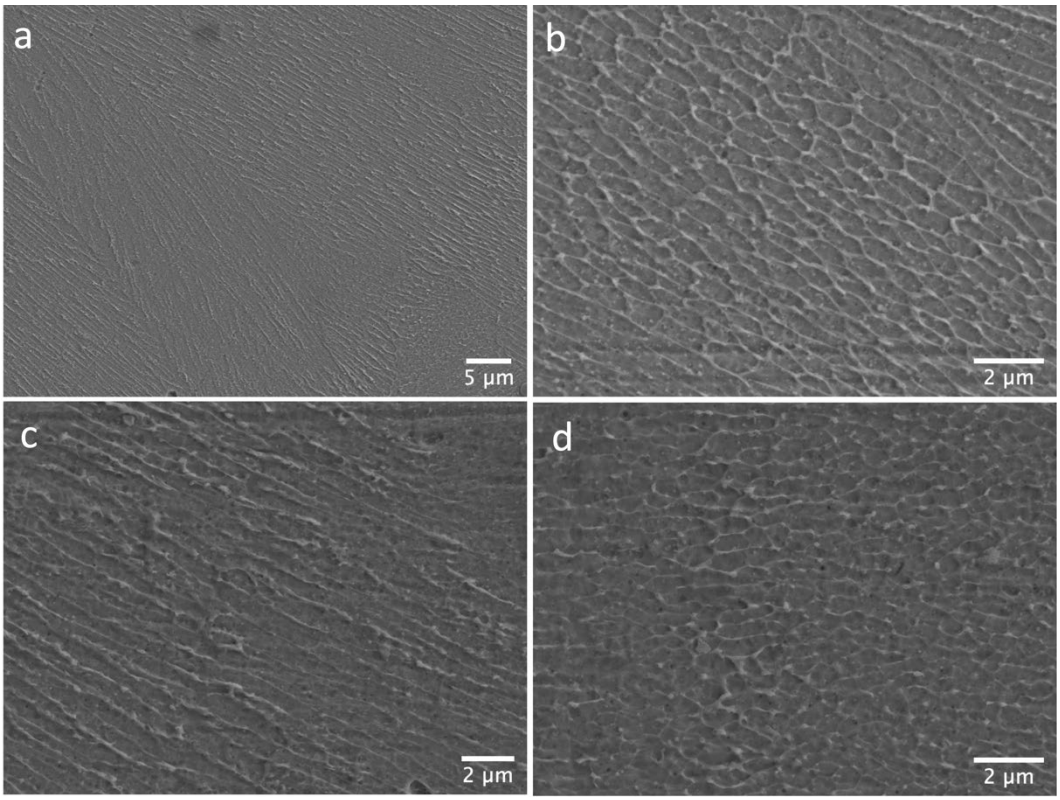

Figure 6. Cellular structure of as-printed ODS SS316L. (a) molten pool boundary, (b) sub-grain in Chessboard pattern sample, (c) molten pool boundary, and sub-grain in Meander pattern sample

3.4 Microhardness

The hardness of as-printed SS316L is influenced by various factors, including grain size, residual stress, and oxide particles. Previous studies have demonstrated that the average hardness of additively manufactured SS316L is 195.4 HV, with a strong correlation to the formation of porosity.[17] Tucho et al. [18] reported an increase in hardness followed by a decrease in hardness with increasing energy density, attributed to the formation of gas-trapping pores. Hardness values ranging from 176 to 213 HV were observed with energy density increasing from 50 to 80 J/mm³. Figure 7 shows that as-printed ODS SS316L exhibited average hardness values of 254.4 HV and 253.5 HV using the meander and chessboard printing patterns, respectively. These values indicate similar enhanced hardness compared to the original SS316L, with minor differences between the samples. This consistency in hardness between the patterns aligns with the observations made through optical microscope characterization. The energy density of 48.5 J/mm³ in this study demonstrates the enhanced microhardness of ODS SS316L can be attributed to the combination of a fine grain structure and dispersion strengthening effects. Firstly, the fine grain structure of SS316L contributes to higher strength based on the Hall-Petch relationship. Muley et al. [19] reported increased hardness in forged SS316L as the grain size was reduced from 30 to 0.86 µm. Additionally, Grandhi et al.[8] observed a fine grain structure in additively manufactured ODS SS316L (with 0.5% Y_2O_3) with the presence of nano inclusions in the matrix, resulting in an elevated hardness value of 3.9 GPa. Furthermore, the dispersion of oxides can impede the

movement of dislocations and grain boundaries, a phenomenon known as oxide dispersion strengthening (ODS) effects in ODS alloys.[6, 20]

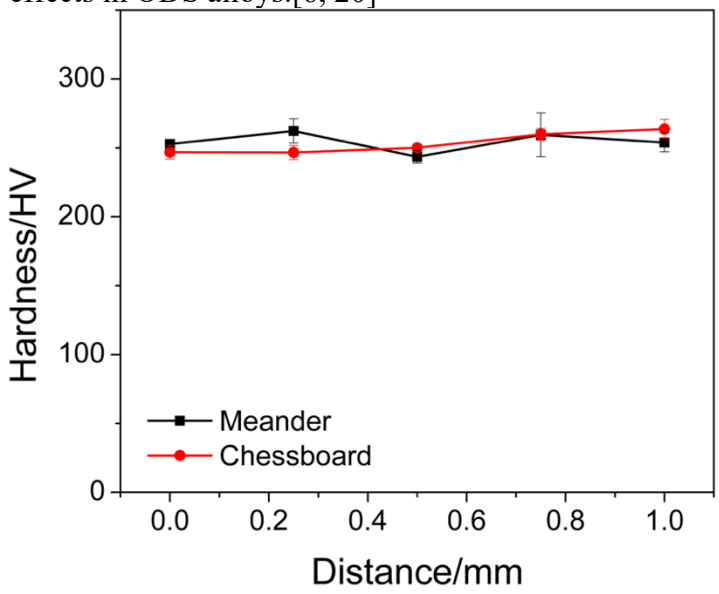

Figure 7. Microhardness of ODS SS316L with meander and chessboard patterns, X axis shows the distance of 0.25 mm between indents.

4. Conclusions and future work

In this study, we successfully produced nano-size Y_2O_3 embedded spherical SS316L powder for laser powder bed fusion additive manufacturing, the main conclusions are as follows:

1. The SS316L powder maintained its spherical shape during the powder processing, and the nano-sized Y_2O_3 particles were uniformly coated onto the host particles without visible Y_2O_3 particles on the powder surface. The produced ODS SS316L powder exhibited a smooth surface compared to the as-received powder, and the particle size distribution ranged from 5 to 40 μm.

2. The powder feedstock was successfully printed using both chessboard and meander patterns, and cellular structures were observed in the as-printed samples. The formation of cellular structures is attributed to the extremely high cooling rate in the L-PBF process. No visible lack of fusion defects was observed in the as-printed ODS SS316L, indicating excellent flowability and laser absorption rate of the powder.

3. The dispersion of oxides in the matrix is an important aspect to investigate. The uniform distribution of oxides would benefit the grain refinement and mechanical properties of the L-PBF-fabricated ODS SS316L. However, the rapid solidification and uneven liquid flow in the process tend to bring oxides to the border of the molten pool, resulting in the formation of coarser oxides in the matrix. Future research should consider proper measures related to the powder feedstock and printing parameters to control the oxide dispersion behavior in L-PBF-fabricated ODS SS316L.

4. As-printed ODS SS316L exhibited average hardness values of 254.4 and 253.5 HV, attributed to the grain refinement and oxide dispersion strengthening (ODS) effects.

The study of L-PBF-fabricated ODS SS316L is still in its preliminary stage, and achieving ultrafine oxides along the molten pool boundary remains a challenge in the L-PBF process. In future research, optimization of the powder feedstock and printing parameters should be undertaken to tailor the oxide dispersion behavior in L-PBF-fabricated SS316L.

Acknowledgements

This work was mainly funded by the U.S. NASA MUREP High Volume project (Award Number 80NSSC22M0132). The author also expresses sincere gratitude to Dr. Marcela Redigolo at West Virginia University for the help on TEM characterization.

References

[1] G. Kalinin, V. Barabash, A. Cardella, J. Dietz, K. Ioki, R. Matera, R.T. Santoro, R. Tivey, Assessment and selection of materials for ITER in-vessel components, Journal of Nuclear Materials 283-287 (2000) 10-19.
[2] J.S. Benjamin, Dispersion strengthened superalloys by mechanical alloying, Metallurgical Transactions 1(10) (1970) 2943-2951.
[3] L. Zhang, S. Ukai, T. Hoshino, S. Hayashi, X. Qu, Y2O3 evolution and dispersion refinement in Co-base ODS alloys, Acta Mater 57(12) (2009) 3671-3682.
[4] R. Allavikutty, P. Gupta, T.S. Santra, J. Rengaswamy, Additive manufacturing of Mg alloys for biomedical applications: Current status and challenges, Current Opinion in Biomedical Engineering 18 (2021) 100276.
[5] B. Li, B.D. Hesar, Y. Zhao, L. Ding, Design and additive manufacturing of porous titanium scaffolds for optimum cell viability in bone tissue engineering, Proceedings of the Institution of Mechanical Engineers, Part B: Journal of Engineering Manufacture 0(0) 0954405420937565.
[6] M.B. Wilms, S.-K. Rittinghaus, M. Goßling, B. Gökce, Additive manufacturing of oxide-dispersion strengthened alloys: Materials, synthesis and manufacturing, Progress in Materials Science 133 (2023) 101049.
[7] Y. Zhong, L. Liu, J. Zou, X. Li, D. Cui, Z. Shen, Oxide dispersion strengthened stainless steel 316L with superior strength and ductility by selective laser melting, Journal of Materials Science & Technology 42 (2020) 97-105.
[8] M. Grandhi, C. Ma, Z. Liu, B. Kang, Microstructural Characterization and Properties of Laser-DED Built Oxide Dispersion Strengthened SS 316 L, Manufacturing Letters 33 (2022) 758-764.
[9] Z. Hu, K. Guan, Z. Qian, J. Dong, J. Wu, Z. Ma, Simultaneous enhancement of strength and ductility in selective laser melting manufactured 316L alloy by employing Y2O3 coated spherical powder as precursor, Journal of Alloys and Compounds 899 (2022) 163262.

[10] I.E. Anderson, E.M.H. White, R. Dehoff, Feedstock powder processing research needs for additive manufacturing development, Current Opinion in Solid State and Materials Science 22(1) (2018) 8-15.
[11] C. Ma, Development of Oxide Dispersion Strengthening (ODS) Alloys Powder for Additive Manufacturing, (2022).
[12] C. Ma, K. Rozman, D. Straub, O. Dogan, S.N. Parbat, M. Chyu, B. Kang, Investigation of Microstructure and Mechanical Properties of Additive Manufacturing Fabricated Oxide Dispersion Strengthening (ODS) IN718 Alloys, Society for Experimental Mechanics Annual Conference and Exposition, Springer, 2022, pp. 75-83.
[13] T.-N. Le, Y.-L. Lo, Effects of sulfur concentration and Marangoni convection on melt-pool formation in transition mode of selective laser melting process, Materials & Design 179 (2019) 107866.
[14] B. Stegman, B. Yang, Z. Shang, J. Ding, T. Sun, J. Lopez, W. Jarosinski, H. Wang, X. Zhang, Reactive introduction of oxide nanoparticles in additively manufactured 718 Ni alloys with improved high temperature performance, Journal of Alloys and Compounds 920 (2022) 165846.
[15] L. Cui, F. Jiang, D. Deng, T. Xin, X. Sun, R.T. Mousavian, R.L. Peng, Z. Yang, J. Moverare, Cyclic response of additive manufactured 316L stainless steel: The role of cell structures, Scripta Materialia 205 (2021) 114190.
[16] P. Deng, M. Karadge, R.B. Rebak, V.K. Gupta, B.C. Prorok, X. Lou, The origin and formation of oxygen inclusions in austenitic stainless steels manufactured by laser powder bed fusion, Additive Manufacturing 35 (2020) 101334.
[17] O. Pannitz, J.T. Sehrt, Transferability of Process Parameters in Laser Powder Bed Fusion Processes for an Energy and Cost Efficient Manufacturing, Sustainability 12(4) (2020) 1565.
[18] W.M. Tucho, V.H. Lysne, H. Austbø, A. Sjolyst-Kverneland, V. Hansen, Investigation of effects of process parameters on microstructure and hardness of SLM manufactured SS316L, Journal of Alloys and Compounds 740 (2018) 910-925.
[19] S.V. Muley, A.N. Vidvans, G.P. Chaudhari, S. Udainiya, An assessment of ultra fine grained 316L stainless steel for implant applications, Acta Biomaterialia 30 (2016) 408-419.
[20] L. Yao, Y. Gao, Y. Li, Y. Huang, Y. Wang, P. Xiao, Q. Liu, Microstructure, mechanical properties, and strengthening mechanisms of nanostructural Y-Zr-O oxide dispersion-strengthened (ODS) Mo alloys, Journal of Alloys and Compounds 921 (2022) 166155.